

## Effect of Mg and Sn Addition on the Corrosion Behavior of an Al-Mn Alloy in 0.5 M H<sub>2</sub>SO<sub>4</sub>

S. Vuelvas<sup>1</sup>, S. Valdez<sup>2</sup>, J. G. Gonzalez-Rodriguez<sup>1,\*</sup>

<sup>1</sup> Universidad Autonoma del Estado de morelos, CIICAp, Av. Universidad 1001, Col. Chamilpa, 62210, Cuernavaca, Morelos, México

<sup>2</sup> Instituto de Ciencias Físicas-UNAM, Av. Universidad S/N, Col. Chamilpa, 062210, Cuernavaca, Morelos, México

\*E-mail: [ggonzalez@uaem.mx](mailto:ggonzalez@uaem.mx)

Received: 29 March 2012 / Accepted: 19 April 2012 / Published: 1 May 2012

---

The effect of Mg addition on the corrosion resistance of an Al-base alloy, nominally AlMgZnMnSn, has been investigated in 0.5 M H<sub>2</sub>SO<sub>4</sub> by using potentiodynamic polarization curves, linear polarization and electrochemical impedance measurements. The addition of Mg to the Al-base alloy cause the precipitation of Al<sub>2</sub>Mg<sub>3</sub>Zn<sub>3</sub> and MgZn<sub>2</sub> precipitates in the grain boundaries. All different techniques have shown that by increasing Mg contents in the alloy the corrosion resistance decreased due to the presence of Al<sub>2</sub>Mg<sub>3</sub>Zn<sub>3</sub> and MgZn<sub>2</sub> precipitates which acted as active anodes. Nyquist diagrams showed that regardless of the Mg contents, the corrosion process is controlled by the adsorption of OH<sup>-</sup> ions. Pitting type of corrosion takes place due to the preferential anodic dissolution of the Al<sub>2</sub>Mg<sub>3</sub>Zn<sub>3</sub> precipitates.

---

**Keywords:** AlMnMgSn alloy, acid corrosion, electrochemical techniques

### 1. INTRODUCTION

Al-Mg based alloys are widely used in aerospace applications due to the unique combination of lightweight and high mechanical properties [1-5]. However, recently Al-Mg alloys have been pointed out as a promising alloy system to be studied due to their low electrode potential, high current capacity to be used as galvanic anode [6]. The application of aluminum and its alloys are often possible because of the natural tendency of aluminum to form a passivating oxide, Al<sub>2</sub>O<sub>3</sub>, layer. However, in aggressive media, the passivating layer can be destroyed, and corrosive attack can take place. A lot of effort has been spent on the investigation about corrosion of Al-alloys [7-25] in many environments, including NaCl [7-15], acidic [16-20] or alkaline solutions [21-25]. Since aluminum is very anodic to the rest of

alloys in most of normally used environments, it will tend to suffer from localized type of corrosion when it is alloyed since different kind of cathodic precipitates are formed.

For instance Birdilis [15] studied the electrochemical behavior and localized corrosion associated with Al<sub>7</sub>Cu<sub>2</sub>Fe particles of 7075 aluminum alloy in NaCl solution, finding that the presence of these particles leads to the development of pitting at the particle-matrix interface. It is known that by alloying with Mg, an increase of this element in Al-Mg alloys significantly increases the strength of the alloy without substantial impact on formability. However, an increase in the Mg contents leads to increase the presence of Al<sub>3</sub>Mg<sub>2</sub> and Mg<sub>5</sub>Al<sub>8</sub> particles in the alloy, which are anodic as compared to the surrounding aluminum matrix, and represents the places where initial corrosion attack takes place. Similarly, Vrsalovic [26] found that the susceptibility towards localized type of corrosion for Al-2.5Mg alloy is higher than that for Al-0.8Mg alloy in 3.5 NaCl solution. Alternatively, Baldwin [7] found that by increasing the Mg content from 2-20% in an Al-Mg alloy, the corrosion current density increases in a saline environment. Thus, the aim of this paper is to have an insight on the effect of Mg addition on the corrosion behavior of an Al-base alloy modified with Sn in an acidic environment by using electrochemical techniques.

## 2. EXPERIMENTAL PROCEDURE

Chemical composition of used alloy is given on table 1, where it can be seen that Mg contents are 3, 20 and 30% respectively.

**Table 1.** Chemical composition of AlMnZn-(Mg) alloy under study (wt.%).

| Alloy  | Al   | Mg   | Zn  | Mn   | Sn   |
|--------|------|------|-----|------|------|
| 3% Mg  | 90.2 | 3.1  | 5.3 | 0.31 | 0.11 |
| 20% Mg | 89.3 | 19.8 | 5.3 | 0.31 | 0.13 |
| 30% Mg | 63.7 | 30.4 | 5.3 | 0.30 | 0.12 |

The alloys were prepared by casting from commercial purity materials. Alloying elements contents were analyzed by using ICP method. Samples were sectioned longitudinally at mid-width using a band saw. One side was prepared for microstructural characterization by using standard metallographic techniques and observed with a scanning electron microscope (SEM). Corrosion tests were performed in 0.5 M H<sub>2</sub>SO<sub>4</sub> solution at 25 °C prepared with analytical reagents. Electrochemical techniques employed included linear potentiodynamic polarization curves, linear polarization resistance, LPR, and electrochemical impedance spectroscopy measurements, EIS, Measurements were obtained each one separately by using a conventional three electrode glass cell with two symmetrically distributed graphite counter electrodes and a saturated calomel electrode (SCE) as reference with a Lugging capillary bridge. Polarization curves were recorded at a constant sweep rate of 1 mV s<sup>-1</sup> at the interval from -500 to +1000 mV with respect to the open circuit potential, E<sub>corr</sub>. LPR measurements

were carried out by polarizing the specimen from +10 to -10 mV respect to  $E_{\text{corr}}$ , at a scanning rate of  $1 \text{ mV s}^{-1}$  every 20 minutes during 24 hours. Electrochemical impedance spectroscopy tests were carried out at  $E_{\text{corr}}$  by using a signal with amplitude of 10 mV and a frequency interval of 0.1 Hz-30 kHz. An ACM potentiostat controlled by a desk top computer was used for the LPR tests, whereas for the EIS measurements, a model PC4 300 Gamry potentiostat was used.

### 3. RESULTS AND DISCUSSION

Fig. 1 shows the X-ray diffraction patterns taken of the Al base specimens. This figure shows that the alloys are composed of  $\alpha$ -Al solid solution,  $\text{MgZn}_2$  and  $\tau$ - $\text{Al}_2\text{Mg}_3\text{Zn}_3$  precipitates when the Mg addition is increased.

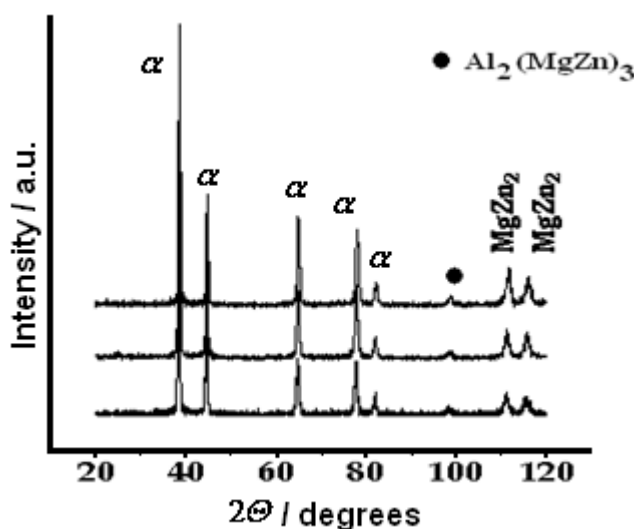


**Figure 1.** X-ray pattern of the AlMnZnMg alloys under study.

One phase precipitation is suggested by the progressive shifting of (530) y (100) X-ray diffraction peaks of  $\alpha$ -phase, from  $2\theta$  angles of  $36.71$ - $35.3^\circ$  y  $8.80$ - $6.58^\circ$ , formed with the alloy containing Mg. The X-ray diffraction patterns show that  $\tau$ - $\text{Al}_2\text{Mg}_3\text{Zn}_3$  and  $\text{MgZn}_2$  precipitates are formed at high Mg addition but there are few reflections of the  $\tau$  precipitates for the low Mg sample. These observations demonstrate that the formation of the  $\tau$ -phase particles was promoted through the high Mg addition. It is apparent also from inspection of Fig. 1 that the relative intensities for the (111) reflection of the  $\alpha$ -Al (which is a rich aluminum solid solution of crystalline structure fcc) is much higher than the other peaks, thereby indicating the presence of a texture was developed during the casting operation.

Fig. 2 shows the microstructure of the as-cast alloys. It can be observed that dendritic structure is broken down and show a quasi-binary eutectic mixture of Al and  $\text{Al}_2\text{Mg}_3\text{Zn}_3$  are present along the grain boundaries of primary  $\alpha$ -Al grains (Fig. 2a).

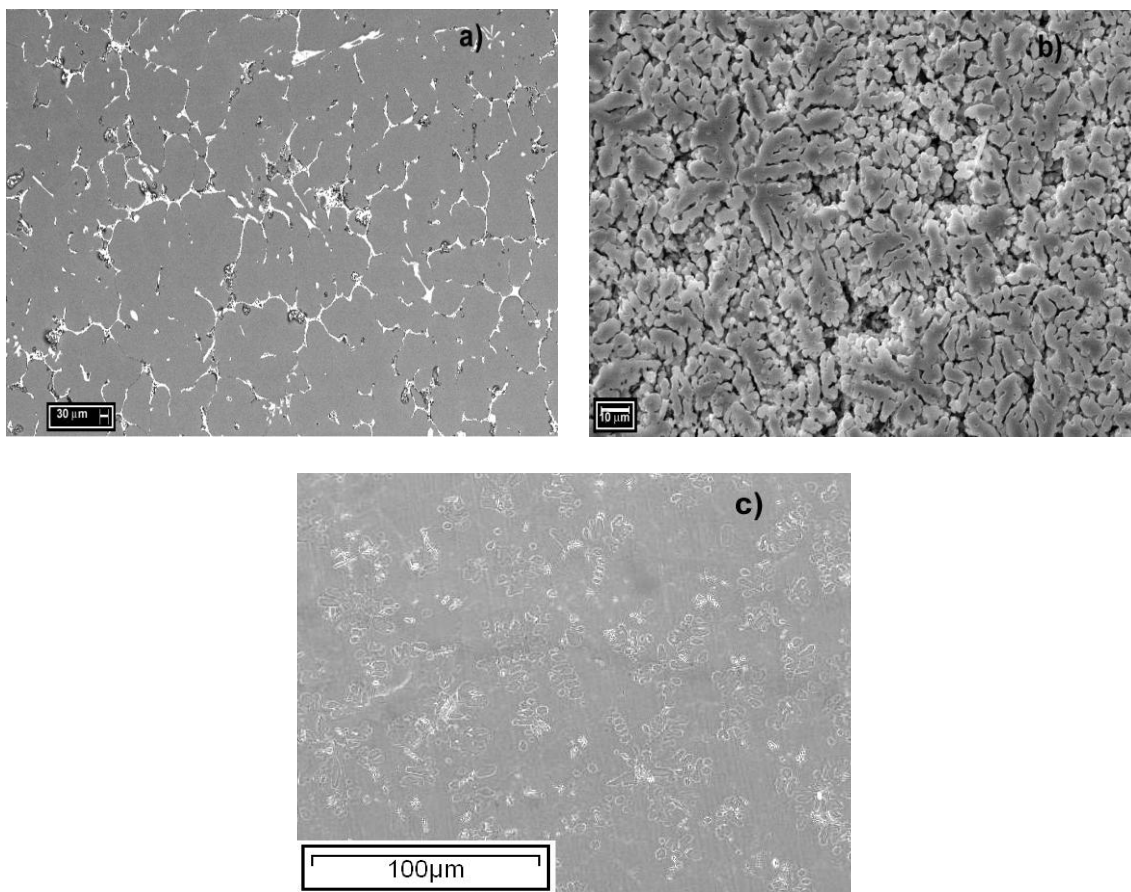


**Figure 2.** Micrographs showing microstructures of the AlMnZnMg alloys containing a) 3, b) 20 and c) 30% Mg.

In the eutectic region the light contrast corresponds to  $\text{Al}_2\text{Mg}_3\text{Zn}_3$ , while dark contrast corresponds to the  $\alpha$ -Al phase. It has been reported [2] that the lamellar eutectic structure is derived from the decomposition of the  $\alpha'$  phase by the following cellular reaction at 762 K,  $\alpha' \rightarrow \alpha + \tau$ - $\text{Al}_2\text{Mg}_3\text{Zn}_3$  ( $\alpha'$  bcc,  $a = 1.416$  nm, Im3). Homogeneously dispersed stable  $\tau$  rods precipitates of 3  $\mu\text{m}$  length in aged samples were observed (Fig. 2a). The literature on alloys [12, 13] of the alloy studied in this work, point out that the equilibrium situation involves the existence of an aluminum based  $\alpha$ -solid solution and another phase ( $\tau$ ) having a variable composition around the  $\text{Al}_2\text{Mg}_3\text{Zn}_3$  formula. The microstructure of the alloy containing 20% Mg (Fig. 2b) reveals the presence of equiaxed dendritic structure with dendrite arm spacing about 20-30  $\mu\text{m}$ . The image presents a dendritic structure characterized by branches and sub-branches of major thickness than the dendritic trunk. In addition, the formation of secondary phases between the dendrite arms is not observed. Another important point of mentioning is the independency of primary and some secondary arms from the dendrite base. When

the magnesium content increases up to 30% wt., Fig. 2 c, the dendritic structure tends to disappear, leaving touches of his existence, due to the probable dendritic structure with poor secondary arms only. Likewise, the absence of interdendritic or precipitate phases is clear.

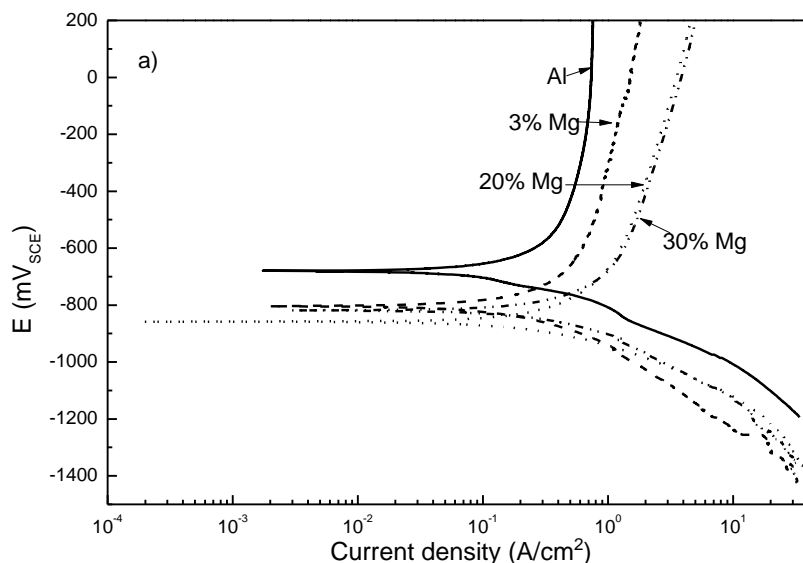


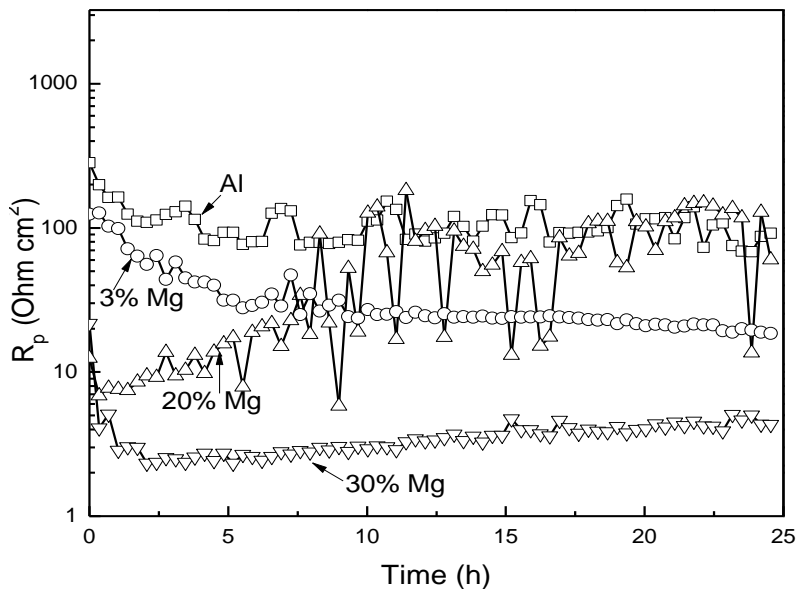
**Figure 3.** Effect of Mg-contents on the polarization curves for AlMnZn alloys in a) 0.5 M H<sub>2</sub>SO<sub>4</sub> and b) 0.5M NaOH.

The effect of Mg addition to the Al-based alloy on polarization curves is shown on Fig. 3. For comparison, a test on pure Al has been included. It can be seen that all materials showed an active-passive behavior, with the anodic current density increasing with the applied potential in the anodic side, until reaching an anodic limit current density, where the current density remained constant with any further increase in the applied potential. The noblest  $E_{corr}$  value, -678 mV, was for unalloyed pure Al, together with the lowest  $I_{corr}$  value, 0.35 A/cm<sup>2</sup>. The anodic current density increased as the Mg contents in the alloy increased and the  $E_{corr}$  value became more active. Thus, the highest corrosion rate was for the alloy containing 30% Mg, indicating the detrimental effect of Mg addition to Al in its corrosion resistance. Electrochemical parameters obtained from these polarization curves are shown on table 2, where the detrimental effect of Mg addition to pure Al is clear.

**Table 2.** Electrochemical parameters obtained from polarization curves.

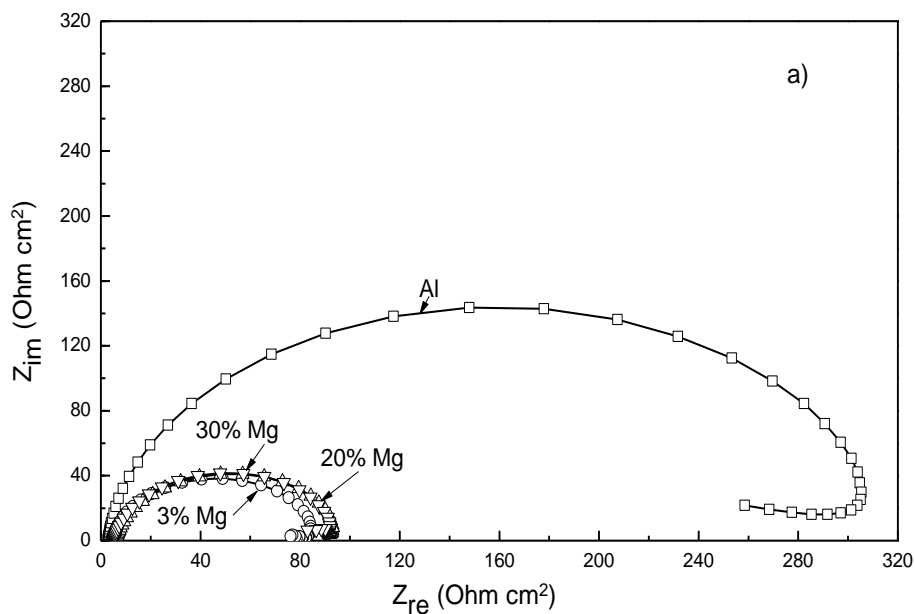
| Alloy  | E <sub>corr</sub> (mV) | I <sub>corr</sub> (A/cm <sup>2</sup> ) | ba (mV/dec) | bc (mV/dec) |
|--------|------------------------|--|-------------|-------------|
| Al     | -678                   | 0.35                                   | 592         | 203         |
| 3% Mg  | -800                   | 0.51                                   | 576         | 250         |
| 20% Mg | -822                   | 0.91                                   | 554         | 273         |
| 30% Mg | -858                   | 0.98                                   | 581         | 189         |

The long-term behavior of the addition of Mg to the Al-base alloy can be seen on Fig. 4, where the change in the polarization resistance value,  $R_p$ , as time elapses is shown. It can be seen from this figure that the highest  $R_p$  value, and thus, the lowest corrosion rate, was for unalloyed Al, although after 10 hours or so, the  $R_p$  value for the alloy containing 20% had similar  $R_p$  values.



**Figure 4.** Effect of Mg-contents on the variation of the  $R_p$  values with time for AlMnZn alloys in 0.5 M  $H_2SO_4$ .

The lowest  $R_p$  value, and thus, the highest corrosion rate, was for the alloy containing 30% Mg, as indicated by polarization curves, Fig. 3.



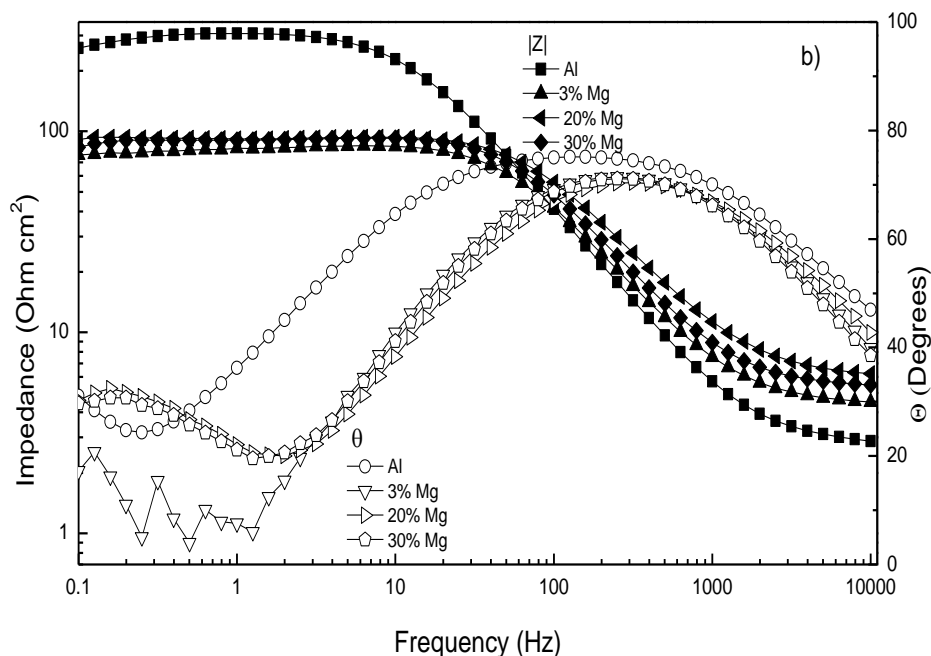


**Figure 5.** Impedance data in the a) Nyquist and b) Bode format for AlMnZnMg alloys in 0.5 M H<sub>2</sub>SO<sub>4</sub>.

Most of the alloys exhibited a trend to decrease the  $R_p$  values as time elapsed to reach a steady state value after a few hours, indicating a stable protective, external passive layer. Alloy containing 20% Mg showed  $R_p$  values increasing with time, indicating a more protective, stable, adherent external passive layer than that formed in the rest of the alloys.

Impedance data in both Nyquist and Bode formats are shown on Fig. 5 a and b respectively. Nyquist plots for all alloys show a capacitive-like semicircle at high and intermediate frequency values which correspond to a charge transfer mechanism from the alloy to the environment to the double electrochemical layer; a second inductive semicircle is observed at lower frequencies. The diameter of the capacitive semicircle corresponds to the charge transfer resistance,  $R_{ct}$ , and is much bigger for pure Al than that for the Mg-containing alloys. The charge transfer resistance,  $R_{ct}$ , is equivalent to the polarization resistance value,  $R_p$ , thus, Nyquist diagrams in Fig. 5 a indicate that pure Al has a higher corrosion resistance than that for the Mg-containing alloys, just as evidenced by polarization curves, Fig. 3 and  $R_p$  values, Fig. 4. The inductive loop observed at low frequency values correspond to an adsorption-controlled corrosion mechanism. This can be due to the fact that the presence of anodic phases, such as the  $Al_2Mg_3Zn_3$  particles shown on Fig. 1, during the alloy formation enhances the susceptibility of hydrolysis reaction. Once hydrolysis reaction starts corrosion reaction can proceed by oxidation of Mg as  $Mg^{2+}$  and Al as  $Al^{3+}$  resulting in the formation of  $Mg(OH)_2$  as follows:



or



The  $\text{Mg}^{2+}$  and  $\text{Al}^{3+}$  ions generate after oxidation of Mg ( $\text{Mg} \rightarrow \text{Mg}^{2+}$ ,  $\text{Al} \rightarrow \text{Al}^{3+}$ ) while  $\text{OH}^-$  releases after oxygen reduction:



Because of insolubility of  $\text{Mg}(\text{OH})_2$  and  $\text{Al}(\text{OH})_3$  in the solution they accumulate at the metal/solution interfaces of the electrode resulting in the formation of corrosion products layer [27-29]. Formation of  $\text{Mg}(\text{OH})_2$  and  $\text{Al}(\text{OH})_3$  with the increase of potential in the anodic region and their subsequent accumulation at the electrode interfaces seems to be the main reason for the occurrence of the diffusion limiting behaviour in the anodic region of the base alloy polarization curves observed on Fig. 3.

On the other hand, Bode diagram, Fig. 5 b, shows that the impedance value is higher for pure Al than that for the Mg-containing alloys, which showed similar impedance values. On the other hand, Bode-phase diagrams show that in all cases there are two time constants; a highly capacitive behavior, typical of passive materials, is indicated from medium to low frequencies by phase angles approaching  $90^\circ$ , suggesting that a very stable film is formed on all tested alloys in the used electrolyte. This passive film is the responsible for the anodic limit current density observed in the polarization curves, Fig. 3. This passive film can be disrupted by aggressive ions, e.g. sulphate ions, and initiate a localized type of corrosion, as shown on Fig. 6, which shows micrographs of the Mg-containing alloys, where it can be seen that the anodic  $\text{Al}_2\text{Mg}_3\text{Zn}_3$  and  $\text{MgZn}_2$  particles have been dissolved. This can be explained in terms of a galvanic effect, since the  $\text{Al}_2\text{Mg}_3\text{Zn}_3$  and  $\text{MgZn}_2$  particles are more anodic than the Al matrix, which acts as cathode, inducing to the preferential dissolution of the  $\text{Al}_2\text{Mg}_3\text{Zn}_3$  and  $\text{MgZn}_2$  particles.

As it was shown by polarization curves, the anodic current density increased as the Mg addition increased. Similar to this study, Birdilis [15] studied the electrochemical behavior and localized corrosion associated with  $\text{Al}_7\text{Cu}_2\text{Fe}$  particles in aluminum alloy 7075 in NaCl solution, finding that the presence of these particles leads to the development of pitting at the particle-matrix interface. It is well known the fact that an increase in the Mg contents leads to increasing the presence of  $\text{Al}_3\text{Mg}_2$  and  $\text{Mg}_5\text{Al}_8$  particles in the alloy, which are anodic as compared to the surrounding aluminum matrix, and represent the places where initial corrosion attack takes place. Thus, the presence of  $\text{Al}_2\text{Mg}_3\text{Zn}_3$  and  $\text{MgZn}_2$  particles in our alloy brings an increase in the corrosion rate not only because of the presence of these anodic sites, but also because of the relation cathode-to-anode area, since we are in presence of a big cathode, the surrounding matrix, and a small anode, the  $\text{Al}_2\text{Mg}_3\text{Zn}_3$  and  $\text{MgZn}_2$  particles. In the SEM observations, it was observed that the microstructure of the alloys consisted of  $\tau$ - $\text{Al}_2\text{Mg}_3\text{Zn}_3$  and  $\text{MgZn}_2$  precipitates surrounded by eutectic  $\alpha$ -aluminum phase. The  $\alpha$ -Al phase is more cathodic, then corrosion occurs in the anodic  $\text{Al}_2\text{Mg}_3\text{Zn}_3$  and  $\text{MgZn}_2$  precipitates as observed in SEM images of

corroded surfaces, Fig.6.  $\text{Al}_2\text{Mg}_3\text{Zn}_3$  and  $\text{MgZn}_2$  precipitates at grain boundaries, and corrosion occurs in the form of pitting in presence of aggressive  $\text{SO}_4^{2-}$  ions.

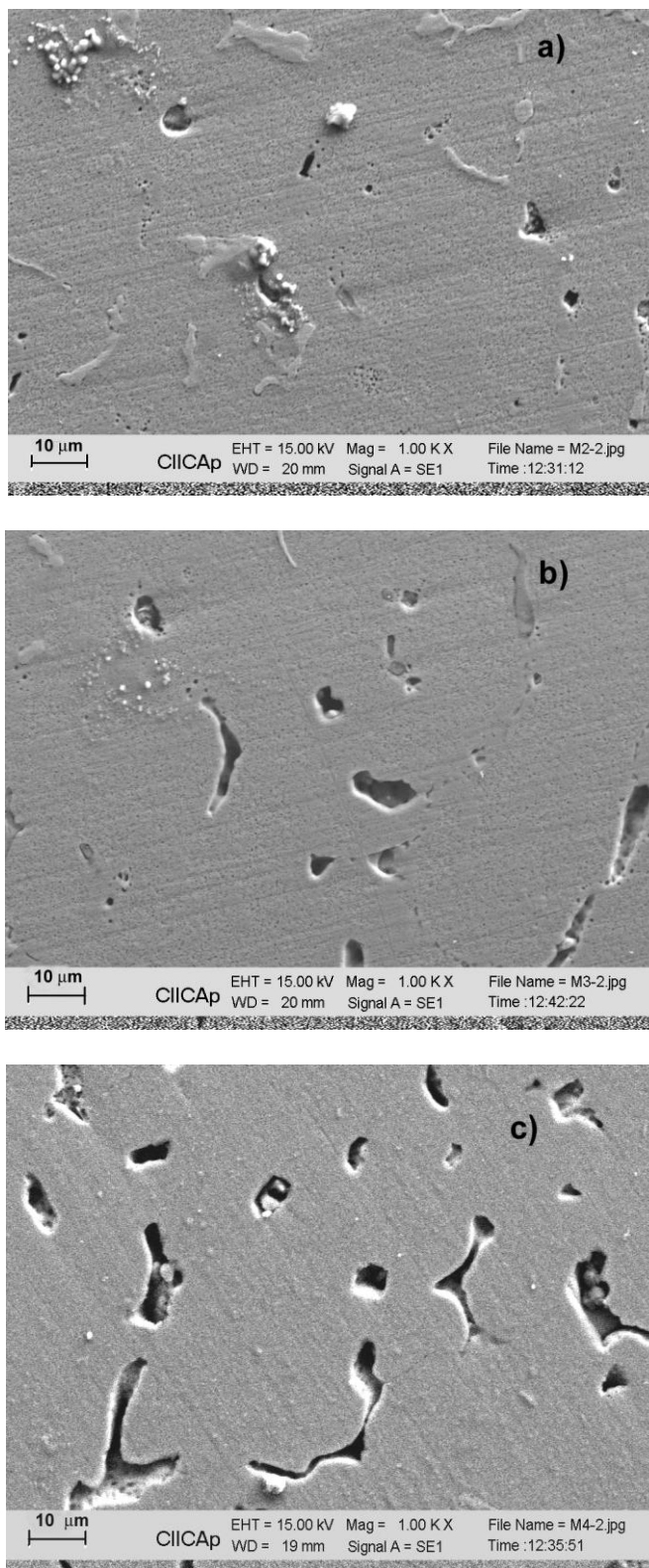


**Figure 6.** Micrographs of the corroded surfaces of the AlMnZnMg alloys containing a) 3, b) 20 and c) 30% Mg in 0.5 M  $\text{H}_2\text{SO}_4$ .

LPR results showed that, during a long part of the experiment, the  $R_p$  value decreased as the Mg content in the alloy increased, decreasing, this way, the corrosion resistance. When nobler elements such as Cu or Si have been added to Al-base alloys, either Cu- or Si-rich cathodic precipitates have been found and the surrounding Al-rich matrix is corroded, showing higher  $R_p$  values than Al-pure alloys [29]. Thus, the decrease in the  $R_p$  value as the Mg contents of our alloy can be explained by the presence of  $Al_2Mg_3Zn_3$  and  $MgZn_2$  precipitates. Impedance measurements showed that the Mg-containing alloys had a smaller semicircle diameter, from 220 ohm  $cm^2$  which corresponds for pure Al, to 90 ohm  $cm^2$  for the alloy containing 30% Mg. The semicircle diameter represents the charge transfer resistance,  $R_{ct}$ , which is equivalent to the polarization resistance value,  $R_p$ , indicating, this way, a decrease in the corrosion resistance as the Mg-contents in the alloy was increased. However, Nyquist diagrams have shown that regardless the Mg-contents, the corrosion process is under control of the adsorption of OH species.

#### 4. CONCLUSIONS

A study of the effect of Mg addition on the corrosion resistance of an Al-base alloy modified with Sn in 0.5 M  $H_2SO_4$  has been carried out by using electrochemical techniques. The addition of Mg to the Al-base alloy cause the precipitation of  $Al_2Mg_3Zn_3$  and  $MgZn_2$  precipitates in the grain boundaries. With increasing Mg content, the amount of these precipitates increases. The electrochemical parameters obtained from polarization curves showed that by increasing Mg contents, the corrosion current density increased. The magnitude of the polarization resistance value,  $R_p$ , decreased with increasing the Mg contents, decreasing, thus, the corrosion resistance of the Al-base alloy. Nyquist diagrams showed that regardless of Mg contents, the corrosion process is controlled by the adsorption of OH<sup>-</sup> ions. Pitting type of corrosion takes place due to the preferential anodic dissolution of the  $Al_2Mg_3Zn_3$  precipitates.

#### References

1. A.V. Sameljuk, O.D. Neikov, A.V. Krajnikov, Y.V. Milman, G.E. Thompson, X. Zhou, *Corros. Sci.*, 49 (2007) 276.
2. F. Mondolfo, *Rev. Metall.* 16 (1971) 953.
3. E.H. Hollingsworth, H.Y. Hunsicker (eds) *Metals Handbook*. ASME, Ohio, 1987.
4. H. Cordier, C. Dumond, W. Gruhl, *Metallurgy* 34 (1980) 515.
5. J. Polmear, *J Inst Met* 89 (1960) 51.
6. A.Barbucci G. Cerisola, G. Bruzzone, A. Saccone, *Electrochim. Acta* 42 (1997) 2369.
7. K.R. Baldwin, R.I. Bates, R.D. Arnell, C.J.E. Smith, *Corros. Sci.* 38 (1996) 155.
8. R. Grilli, M. A. Baker, J. E. Castle, B. Dunn, J. F. Watts, *Corros. Sci.* 52 (2010) 2855.
9. C. Blanc, G. Mankowski, *Corros. Sci.* 39 (1997) 959.
10. A.S. Handy, *Mater. Lett.* 60 (2006) 2633.
11. J. Hu, Y.B. Li, H.L. Wang, W.C. Rend, *Mater. Lett.* 62 (2008) 715.
12. S. Gudic, I. Smoljko, S. Kliskie, *Mater. Chem. Phys.* 121 (2010) 561.
13. M. Elboudjaini, E. Ghali, R.G. Barradas, M. Girgis, *J. Appl. Electrochem.* 25 (1995) 412.

14. R.S. Chaudhary, P.N.S. Yadav, C.V. Agarwal, *J. Appl. Electrochem.* 13 (1983) 807.
15. N. Birbilis, M.K. Cavanaugh, R.G. Buchheit, *Corros. Sci.* 48 (2006) 4202.
16. G.O. Avwiri, F.O. Igho, *Mater. Lett.* 57 (2003) 3705.
17. I.B. Obot, N.O. Obi-Egbedi, S.A. Umoren, E.E. Ebenso, *Int. J. Electrochem. Sci.* 5 (2010) 994.
18. I.B. Obot, N.O. Obi-Egbedi, *Int. J. Electrochem. Sci.* 4 (2009) 1277.
19. V. Branzoi, F. Golvovici, F. Branzoi, *Mat. Chem. Phys.* 78 (2003) 122.
20. E.E.F. El-Sherbini, S.M. Abd-El-Wahab, M.A. Deya, *Mater. Chem. Phys.* 82 (2003) 631.
21. M.A. Amin, S.S.A. El-Rehim, E.E.F. El-Sherbini, O.A. Hazzazi, M.N. Abbas, *Corros. Sci.* 51 (2006) 658.
22. E.E. Oguizie, B.N. Okulue, C.E. Ogukwe, C. Unaegbu, *Mater. Lett.* 60 (2006) 3376.
23. A.M. Abdel-Gaber, E. Khamisa, H. Abo-EIDahaba, S. Adeel, *Mater. Chem. Phys.* 109 (2008) 297.
24. M. Boinet, J. Bernard, M. Chatenet, F. Dalard, S. Maximovitch, *Electrochim. Acta* 55 (2010) 3454.
25. D. Chu, R.F. Savinell, *Electrochim. Acta* 36 (1991) 1631.
26. L. Vrsalovic, M. Kliskic, S. Gudic, *Int. J. Electrochem. Sci.* 4 (2009) 1568.
27. T.B. Massalski, *Binary Alloy Phase Diagrams*, ASTM, OH, 1986.
28. S. Zor, M. Zeren, H. Ozkazanc, E. Karakulak, *Anti-Corrosion Methods and Materials* 57 (2010) 185.